CHEMICAL WEARING MECHANISM OF REFRACTORY MATERIALS IN A STEEL LADLE SLAG LINE

R.A. Mattila, J.P. Vatanen and J.J. Härkki

University of Oulu, Laboratory of process metallurgy,
P.O. BOX 4300, FIN-90014 OULUN YLIOPISTO, Finland.
Fax + 358 8 553 2339 Tel. + 358 8 553 1011 Http://cc.oulu.fi/~pometwww/

Key Words: rotating furnace, high temperature corrosion, refractory materials, slag, ladle

ABSTRACT

The goal of this work was to study the wearing mechanism of refractory materials in a steel ladles slag line. The studied refractory materials were MgO-C bricks, doloma brick, corundum castable and spinel castable. Rotating furnace and sessile drop tests were conducted with converter and steel slags. The corrosion index, infiltration zone and refractory/slag mineralogical reactions were studied.

The wear mechanisms of refractory materials were studied using SEM, XRF and XRD analysing techniques and thermodynamic calculations. The driving force behind chemical wearing is chemical potential differences of the components between lining and slag. In general, the main principles of chemical wearing depend on the structure and mineralogical character of the refractory material.

INTRODUCTION

Wearing of the ladle slag line is the biggest refractory material problem with ladles. Chemical, thermal and mechanical wearing occur in the slag line. The chemical potential difference between the components of the refractory material and the slag under high temperature conditions is the driving force behind the chemical wearing mechanism. Usually, chemical wearing does the “groundwork”. Thermal and mechanical wearing finish the job. The refractory material and process conditions determinate what kind of mechanism has the most effective role. We can affect the wearing rate of slag lines through the choice of refractory material, the composition of the slag and temperature control.

The literature presents wearing mechanism for refractories in different conditions than in this research. /1,2,3,4/

The purpose of this research was to find out the chemical wearing mechanisms of refractory materials against test ladle slag and converter slag.

The experimental method used was a rotating furnace test and analysis of the test materials after the test.

PHASE STABILITY CALCULATIONS

Phase stability diagrams were made using the HSC application's Gibbs routine. Some hypothetical assumptions were made. The starting values for the calculation of HSC equilibrium diagrams for ladle slag are shown in table 1 and for converter slag in table 2.

MgO-Carbon brick

Figure 1 shows the phase stability diagram for the reactions between MgO-C brick and ladle slag components. Carbon is not included in the calculations. Calcium oxide reacts with aluminium and silica oxide at low temperatures to form calcium-dialuminate ($CaO{\cdot}2Al_2O_3$), tricalcium-silicate (Ca_3SiO_5) and mayenite ($12CaO{\cdot}7Al_2O_3$). Hercynite ($FeAl_2O_4$) and dicalcium-ferrite ($CaO{\cdot}Fe_2O_3$) can compound at low temperature.

Figure 2 shows the phase stability diagram for the reactions between MgO-C brick and converter slag components. Converter slag reacts to form tricalcium-silicate (Ca_3SiO_5) and calcium-ferrite ($2CaO{\cdot}Fe_2O_3$), which is stable at low temperatures. Calculations show that periclace is stable in all temperature ranges.

Corundum and spinel castables

Figure 3 shows the phase stability diagram for the reactions between spinel castable and ladle slag components. Calcium-dialuminate ($CaO{\cdot}2Al_2O_3$) and tricalcium-silicate (Ca_3SiO_5) are the first stable components to be formed. Hibonite ($CaAl_{12}O_{19}$) and spinel ($MgO{\cdot}Al_2O_3$) start to form at 1400 °C.

Figure 4 shows the phase stability diagram for the reactions between corundum castable and ladle slag components. The phase stability diagram is almost the same asthat of spinel castable, but there is no spinel formation.

Figure 5 shows the phase stability diagram for the reactions between spinel castable and converter slag components. The first phases to be crystallised are hercynite ($FeAl_2O_4$) and tricalcium-silicate (Ca_3SiO_5).

Figure 6 shows the phase stability diagram for the reactions between corundum castable and converter slag components. According to the thermodynamic calculations, the first phases to be crystallised are hercynite ($FeAl_2O_4$) and calcium-dialuminate ($CaO{\cdot}2Al_2O_3$). At 1200 °C dicalcium-ferrite ($2CaO{\cdot}Fe_2O_3$) starts to form and at 1400 °C hibonite ($CaAl_{12}O_{19}$) is formed.

Doloma brick

Figure 7 shows the phase stability diagram for the reactions between doloma brick and ladle slag components. According to the thermodynamic calculations, the first phases to be formed are calcium-dialuminate ($CaO{\cdot}2Al_2O_3$) and tricalcium-silicate (Ca_3SiO_5).

Figure 8 shows the phase stability diagram for the reactions between doloma brick and converter slag components. According to the thermodynamic calculations, the first phases to be formed are dicalcium-ferrite ($2CaO{\cdot}Fe_2O_3$) and tricalcium-silicate (Ca_3SiO_5). Calcium vanadium oxide ($3CaO{\cdot}V_2O_5$) and calcium-titanium oxide ($4CaO{\cdot}3TiO_2$) are stable, in all the temperature ranges.

EXPERIMENTS

Tests were conducted in a rotating furnace. A schematic drawing of the inside of the furnace is shown in figure 9. All the test materials were in the same ring.

The furnace was rotating around its axle at a rate of 4 rotations per minute. The temperature was monitored online by means of a pyrometer on the surface of the second test ring material. The temperature was controlled by altering the rate of flow of oxygen and propane. The test conditions are given in table 3. The bricks were sawn to dimensions and the castables were cast in a mould. The castables were made by following the manufacturer‘s instructions. The chemical and physical properties of the test materials are given in table 4. Genuine process slags were used in the test. Fresh slag was added continuously during the test to keep the chemical potential difference stable. The chemical composition of the ladle and converter slags used in the test is given in the table 5.

A sessile drop test was conducted in a tube furnace in an argon atmosphere. Refractory samples were burned 10 mm*10 mm*4 mm plates and slag was 4 mm*4 mm sylinders.

RESULTS

The relative corrosion rate in the rotating furnace tests is presented in figure 10. The slag penetration depth is presented in figure 11. The test materials were ranked based on these two indexes. The corrosion rate is weighted as more important than the penetration depth.

In the rotating furnace test the corundum castable had the worst durability against the test slags. The doloma brick also had quite unfavourable durability against the test slags. The spinel material had slightly better durability than the first materials. The best materials were MgO-C bricks. Increases in carbon content from 5 % to 14 % give 5 % wearing differences in the rotating furnace tests. MgO-C 14 % brick had the best durability against slag in this test. The difference in the corrosion index between the worst and best material was 25 %.

One weakness of the rotating furnace test is in indicating wearing kinetics. This is because there was no measurement of the wearing rate between the start and the end of the test. The sessile drop method was used for corundum and spinel castables to test their reaction rate. The findings were that after 10 minutes at 1400 °C against ladle slag, all the slag had infiltrated into the corundum castable and almost all into the spinel castable. This indicates that slag penetration into the refractories and reactions between the slag and the refractory material can occur very quickly. The wearing mechanism comparing to the rotating furnace tests seems to be the same based on (SEM, EDS) the analysis of the sessile drop samples.

All the test pieces were analysed after testing by using a scanning electron microscope (SEM) with an energy dispersive spectrometer (EDS) , an x-ray diffractometer (XRD) and an x-ray fluorescence spectrometer (XRF).

Mineralogical and chemical analysis (XRD)
Table 6-8 shows the chemical and mineralogical analysis of the converter slag tests (test 1) and table 9-11 shows the chemical and mineralogical analysis of the ladle slag tests (test 2).

MgO-Carbon bricks after testing against converter slag (SEM, EDS)

Figure 12 shows MgO-Carbon (10 % by weight of C) brick and its reactions with converter slag components. It shows the slag and brick contact zone. The minerals from the lighter area are gehlenite, spinel, iron and dicalcium-silicate ($2CaO \cdot SiO_2$). Figure 13 shows a closer picture of MgO-Carbon brick and its reactions with converter slag components. It is obvious that the iron oxide component of the converter slag has reduced the carbon content of the bricks.

After carbon reduction, slag can penetrate into the brick and surround the periclase grains. Melting and recrystallisation of the penetrated slag components can cause volume changes inside the brick. Those volume changes are due to the temperature differences of the process. Mechanical movement can also cause periclase grains to break off from the matrix. The iron oxide (FeO) content of the periclace grain reaction zone is about 15-20 %.

Spinel castable after testing against converter slag (SEM, EDS)
Figure 14 shows spinel castable reactions with converter slag components. It shows the slag and brick contact zone. Figure 15 shows a closer picture of the contact zone. The minerals from the lighter area are gehlenite, spinel, calcium-dialuminate ($CaO \cdot 2Al_2O_3$) and calcium-iron-aluminate.

Corundum castable after testing against converter slag (SEM, EDS)
Figure 16 shows corundum castable reactions with converter slag components. It shows the slag and mass contact zone and about a 10 mm deep slag infiltration zone. The minerals from the lighter area are spinel, hibonite [$CaO \cdot 6Al_2O_3$], mayenite, and gehlenite [$Ca_2Al_2SiO_7$].

Doloma brick after testing against converter slag (SEM, EDS)
Doloma brick is formed from periclase and calcium oxide. Figure 17 shows doloma brick reactions with converter slag components. It shows the slag and brick contact zone. The minerals from the slag phase are tricalcium-silicate and periclase.

MgO-Carbon bricks after testing against ladle slag (SEM, EDS)
Figure 18 shows MgO-Carbon (10 % C) brick and its reactions with ladle slag components. A spinel layer has been formed next to the MgO-C brick. Figure 19 shows a closer picture of the MgO-Carbon brick and its reactions with ladle slag components. The minerals from the lighter area are spinel, mayenite (C12A7), gehlenite-åkermanite solid solutions in an aluminium-rich phase (MgO 9 %, Al_2O_3 35 %, SiO_2 15 %, CaO 38 %) and dicalcium-silicate ($2CaO \cdot SiO_2$).

Ladle slag is not as aggressive as converter slag. As can be seen from the SEM pictures, there is no periclace grains in the slag. Chemical wearing is not as apparent as with converter slag. The reason for the differences is the slag's iron oxide content.

Spinel castable after testing against ladle slag (SEM, EDS)
Figure 20 shows spinel castable reactions with ladle slag components. A spinel layer has been formed from the slag. Figure 21 shows corundum grain reactions with ladle slag, forming hibonite and calcium-aluminate layers.

Corundum castable after testing against ladle slag (SEM, EDS)
Figure 22 shows corundum castable reactions with ladle slag components. A spinel layer has been formed from the slag. Figure 23 shows corundum grain reactions with ladle slag,

forming dicalsium-silicates, calcium-silicate-aluminate, spinel, mayenite and hibonite. Note that the hibonite and mayenite layers dissolve aluminium from the corundum mass.

Doloma brick after testing against ladle slag (SEM, EDS)
Figure 24 shows doloma brick reactions with ladle slag components. It shows the slag and brick contact zone. X-ray diffractometry analysis indicated the minerals from the slag phase are mayenite and calcium silicate. Doloma is formed from calcium oxide and periclase.

WEAR MECHANISM

The main principle behind chemical wearing in corundum and spinel castables and doloma brick is that the slag dissolves the refractory material up to the component‘s saturation point. One way to control the chemical wearing of corundum and spinel castables is by means of the slag‘s basicity. The chemical wearing of MgO-C bricks is due to carbon reduction of the slag components.

MgO-Carbon brick
The chemical wearing mechanism of MgO-C brick is due to the converter slag‘s iron oxide component‘s reactions with brick carbon, as seen from formula 1.

$$FeO(s) + C(s) = Fe(s) + CO(g) \quad (1)$$

After the carbon loss, slag penetration into the brick is possible. The slag penetrates and surrounds the periclase grains. Now it is possible that the infiltrated slag‘s spalling and mechanical movement can loosen the periclase grains.

The periclase grains dissolve only a little into the slag. At the hot surface the slag‘s iron has reacted with the periclase grains. There is a solid solution of iron oxide and magnesium oxide. The FeO content was up to 15 % at the border of the periclase grains. As can be seen from the phase diagram of FeO_n-MgO, the increasing iron oxide content decreases the melting point of the FeO-MgO solid solution. After all, this fact has no significant role in the wearing mechanism of the MgO-C bricks.

MgO-C bricks have a better durability against ladle slag than converter slag. The main components of ladle slag are CaO, Al_2O_3 and SiO_2, which are not as reducing as the FeO component is. In this case chemical wearing is also due to the carbon reduction of the bricks.

In the test circumstances there was formation of a spinel layer. The formation of spinel has an effect against the brick. The conditions of spinel crystallisation are decreasing temperature (colder brick) and dissolution of magnesium from the periclase grains.

Spinel castable
The composition of converter slag is plotted in an FeO 20 % -Al_2O_3-CaO-SiO_2 phase diagram figure 25. The effect of increasing aluminium content on mineral composition at the slag/refractory reaction zone can been seen from the diagram.

Figure 26 shows how increasing SiO_2 decreases the melting point of the spinel grains. The minerals that are formed are cordierite ($2MgO{\cdot}2Al_2O_3{\cdot}5SiO_2$) and sapphirine ($4MgO{\cdot}5Al_2O_3{\cdot}2SiO_2$). The melting point of cordierite is 1460 °C, and sapphirine decomposes at 1475 °C.

It is obvious that the weakest part of the spinel castable is the matrix. The matrix is formed mainly from < 50 μm corundum and spinel grains. The chemical wearing mechanism of the spinel castable starts with the spinel and ladle slag reaction.

Analysis of the rotating furnace tests show that corundum grains can also dissolve into the slag. The chemical wearing of the corundum grains starts with the formation of the hibonite ($CaO \cdot 6Al_2O_3$) layer. The next mineral to be formed is calcium-dialuminate ($CaO \cdot 2Al_2O_3$). Aluminium cations use the hibonite phase as a passageway to the next layer.

The composition of ladle slag is plotted in an Al_2O_3-CaO-SiO_2 phase diagram figure 27. The effect of increasing aluminium content can be seen from figure 27. Theoretically, it is possible to form all the mineral phases shown in figure 27, increasing aluminium content. Aluminium-rich minerals found in the SEM analysis were hibonite, iron-hibonite, merwinite, kyanite and mayenite. Mayenite ($12CaO \cdot 7Al_2O_3$) and hibonite ($CaAl_{12}O_{19}$) have the most negative $\Delta G°$ values.

Corundum castable

Corundum castable and converter slag chemical wearing are due to the chemical potential differences of the CaO and SiO_2 components between the slag and the mass. The main reason for the worst durability of the corundum castable in these tests was that the corundum castable matrix involves about 1.4 % SiO_2 and 2.5 % CaO. It is not sure in what mineral form CaO and SiO_2 are, but they form the main components in the binding phase. Aggressive converter slags dissolve the corundum mass CaO and SiO_2 compounds. After dissolving, spalling and mechanical wearing can loosen corundum grains. Dissolving FeO decreases the melting point of the calcium-silicates and increases the viscosity of the slag phase. Figure 28 shows the viscosity of melted CaO-Fe_2O_3.

The chemical wearing of the corundum castable and ladle slag is due to the chemical potential differences between CaO and SiO_2 components into the slag and the castable. Ladle slags don't include significant amounts of iron, and that is reason for less violent wearing. The main principle for chemical wearing is the same as the reaction between corundum castable and converter slag.

Doloma brick

The chemical wearing mechanism of doloma bricks is as follows. Wearing starts with the reaction of converter slag FeO, Al_2O_3 and SiO_2 components with the brick`s CaO. The periclase grains are mainly chemically stable during slag infiltration. The slag infiltrates deeply into the doloma brick. SEM analyses show that the infiltration zone contained tricalsium silicate (m.p. 1460 °C) calcium aluminate (m.p. 1605 °C), mayenite (m.p. 1413 °C) and brownmillerite (m.p. 1415 °C).

The dissolution of CaO components with ladle slag components starts the chemical wearing of doloma bricks. The main components of the ladle slags are Al_2O_3, CaO and SiO_2. SEM analyses show that the infiltration zone contained mayenite (m.p. 1413 °C) and calcium silicate (m.p. 1190 °C). The melting points of these minerals are considerably lower than that of converter slag and doloma brick reaction minerals. Figure 29 shows the phase diagram of the CaO-FeO-SiO_2 system and converter slag composition.

Mechanical wearing can loosen periclase grains. Crystallisation and melting of infiltrated slag minerals and their temperature expansion/contraction can make it easier to break off periclase grains.

CONCLUSIONS AND DISCUSSION

The best materials in this test were MgO-C bricks. The best of these was MgO-C 14 %. The main cause of chemical wearing of MgO-C bricks is FeO and other thermodynamically unstable oxides in the slag. Unstable oxides reduces the carbon content of the brick and wearing continues by slag penetration, and the slag surrounds the periclase grains. Now it is possible that infiltrated zone spalling and/or slag flow can dispose periclase grains into the slag.

The chemical wearing of the spinel castable starts with the spinel and ladle slag reaction. SiO_2 decreases melting point of the spinel grains. The minerals that are formed are cordierite ($2MgO{\cdot}2Al_2O_3{\cdot}5SiO_2$) and sapphirine ($4MgO{\cdot}5Al_2O_3{\cdot}2SiO_2$). The melting point of cordierite is 1460 °C, and sapphirine decomposes at 1475 °C.

The dissolutionof the CaO components of doloma bricks with the ladle slag components starts the chemical wearing. the main components of the ladle slags are Al_2O_3, CaO and SiO_2. SEM analysis shows that the infiltration zone contained mayenite (m.p. 1413 °C) and calcium silicate (m.p. 1190 °C)

The chemical wearing of the corundum grains starts with the formation of a hibonite ($CaO{\cdot}6Al_2O_3$) layer. The next mineral to be formed is calcium-dialuminate ($CaO{\cdot}2Al_2O_3$). Aluminium cations use the hibonite phase as a passageway to the next layer.

There is no comparable test in the literature, but the general outline of wearing was quite the same.

The chemical wearing mechanism that was found in the tests also happend in the process. The process conditions can, however, be different, and steel is always included. Based on one sample taken from the ladle slag line after the refractory lining was worn out, the chemical mechanism seems to be the same. Of course, the metal / slag interface seems quite different, but the flow is much stronger in that area because of the margoni effect. This causes the steel/slag/lining point to wear much faster than elsewhere in the slag line area.

All the factories that participated in this project already use MgO-C bricks in the ladle slag line. Focusing on a lining practice like isolation could extend the lifetime of the lining. Just as important is to keep the tapping temperature under control and to avoid converter slag access to the ladle. Converter slag usually contains some FeO, which causes MgO-C wearing. Temperature control is important because very high temperatures cause wearing by the reduction mechanism.

ACKNOWLEDGEMENTS

The financial support provided by Jernkontoret and Rautaruukki Steel is gratefully acknowledged. The authors thank Jaakko Kärjä, Hannu Nevala and Raimo Aho for contributing to this reseach.

REFERENCES

1. H. Barthel, G. Buchebner, E. Kaltner. The magnesia-based lining of oxygen steel converters to conform with changed requirements. Interceram, special issue 1985, 4 p.
2. J. Pierard, Du Siechen, P.Jönsson, S. Seetharaman, T. Landin. Effect of slag on carbon bearing MgO refractories. Ironmaking and steelmaking, 1998, Vol.25, No.5, p. 374-381.
3. B. Nagai, O. Matsumoto, T. Isobe, Y. Nishiumi. Wear mechanism of castable for steel ladle by slag. Taikabutsu overseas, 1990, Vol.12, No.1, p. 15-20.
4. M.H. Tikkanen, K. Lilius, J. Härkki, M. Häikiö. On the reactions of a dolomitic lining in the AOD process. Interceram, special issue 1985, p. 41-44.
5. HSC. Chemistry for windows, version 4.0.
6. Allibert M. et al. Edited by VDEh. Slag atlas. 2nd edition. Düsseldorf 1995. Verlag stahleisen Gmbh. 616 p.

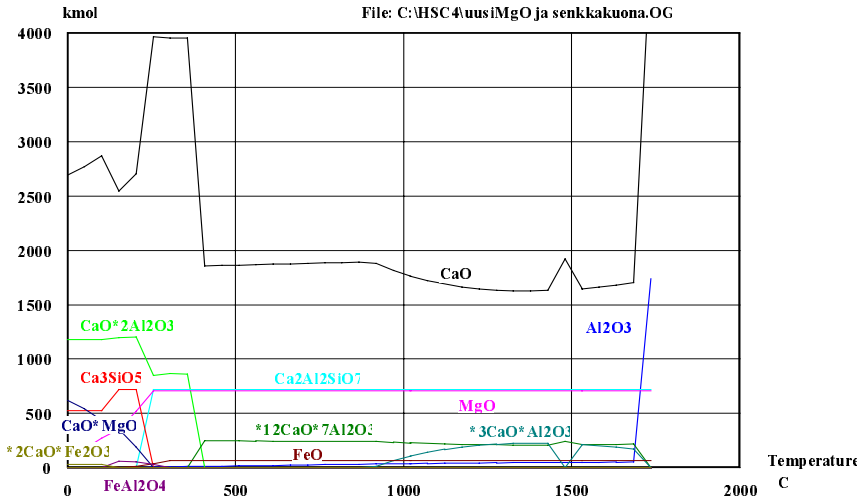

Figure 1. Phase stability diagram. Reactions between MgO-C brick and ladle slag.

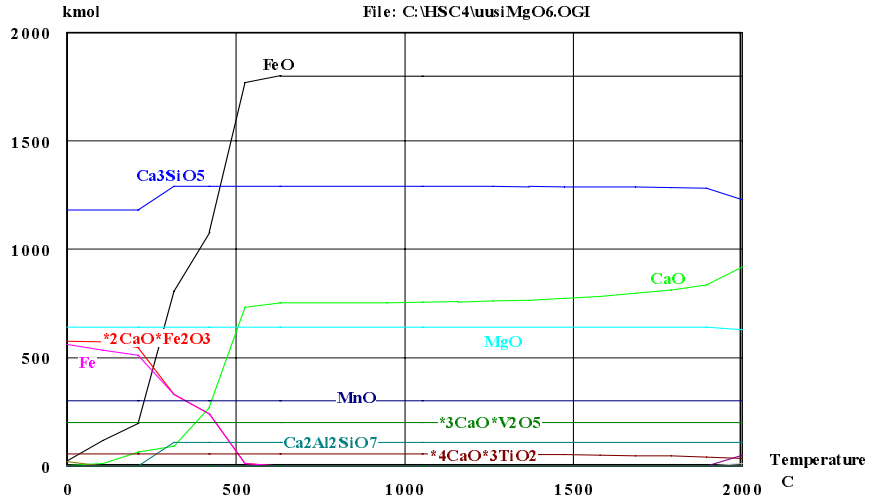

Figure 2. Phase stability diagram. Reactions between MgO-C brick and converter slag.

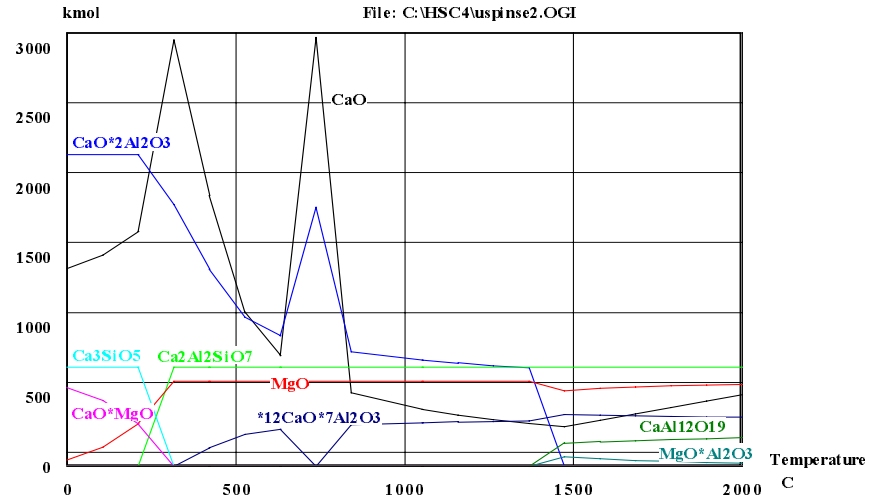

Figure 3. Phase stability diagram. Reactions between spinel castable and ladle slag.

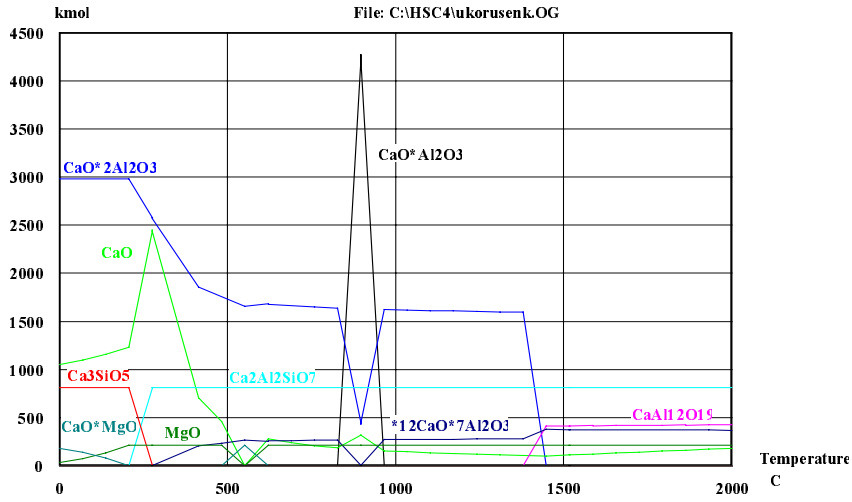

Figure 4. Phase stability diagram. Reactions between corundum castable and ladle slag.

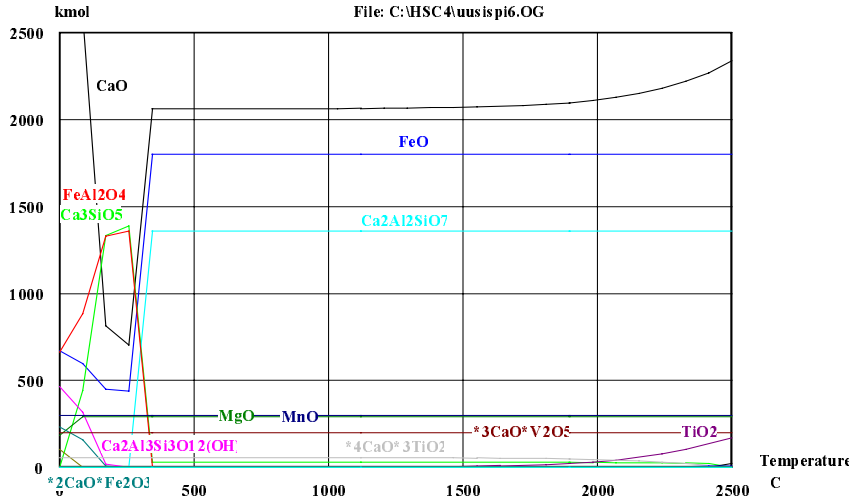

Figure 5. Phase stability diagram. Reactions between spinel castable and converter slag.

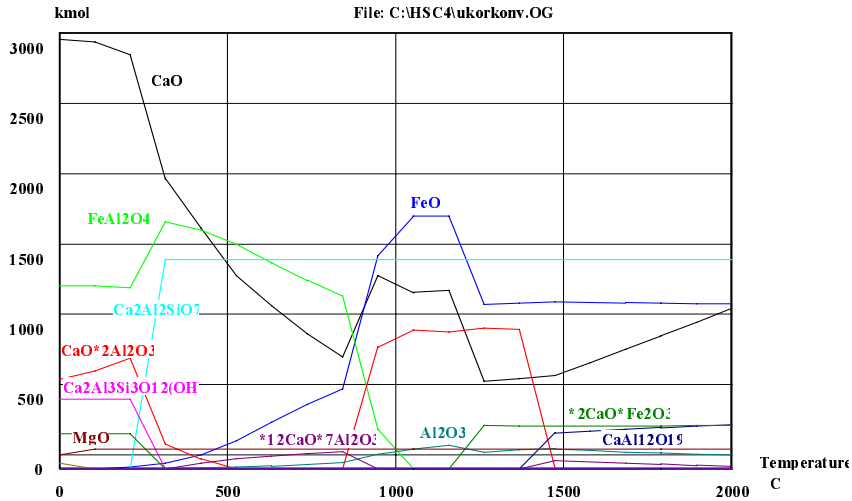

Figure 6. Phase stability diagram. Reactions between corundum castable and converter slag.

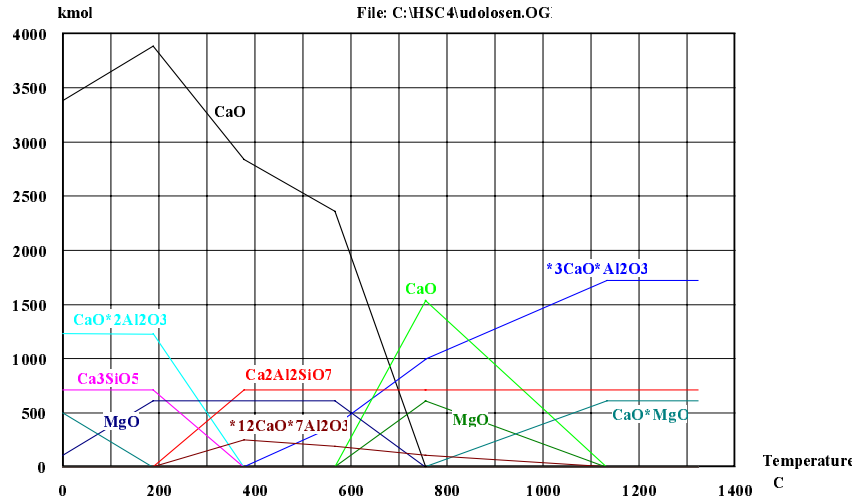

Figure 7. Phase stability diagram.Reactions between doloma brick and ladle slag.

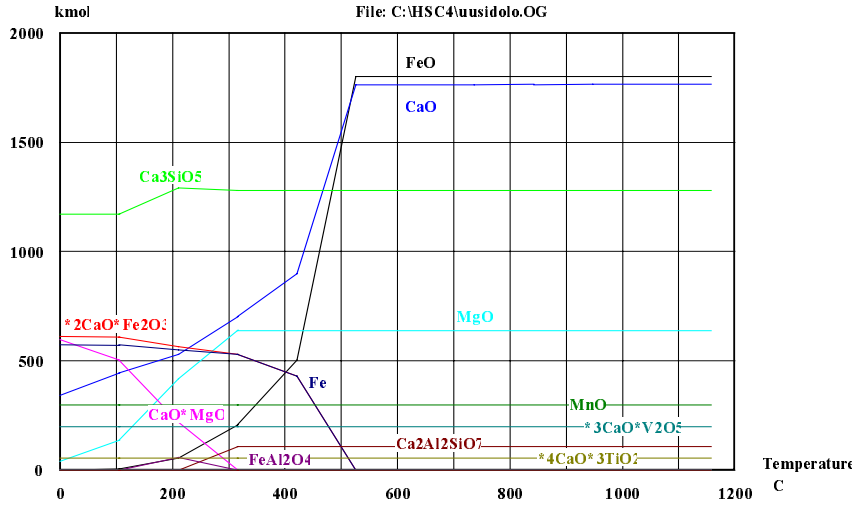

Figure 8. Phase stability diagram. Reactions between doloma brick and converter slag.

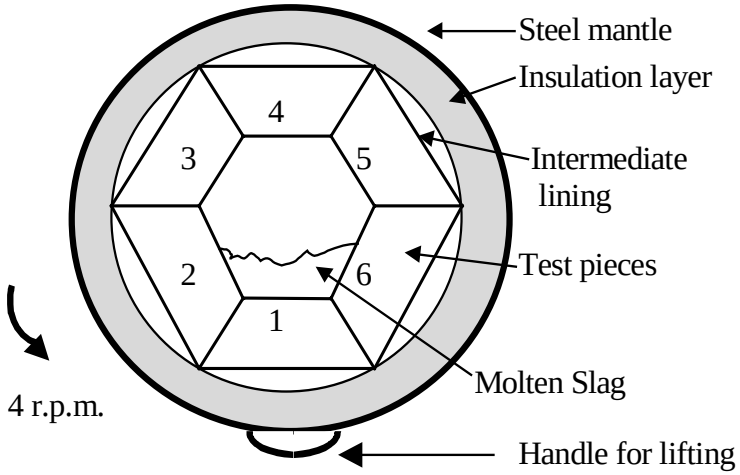

Figure 9. Schematic picture of the rotating furnace.

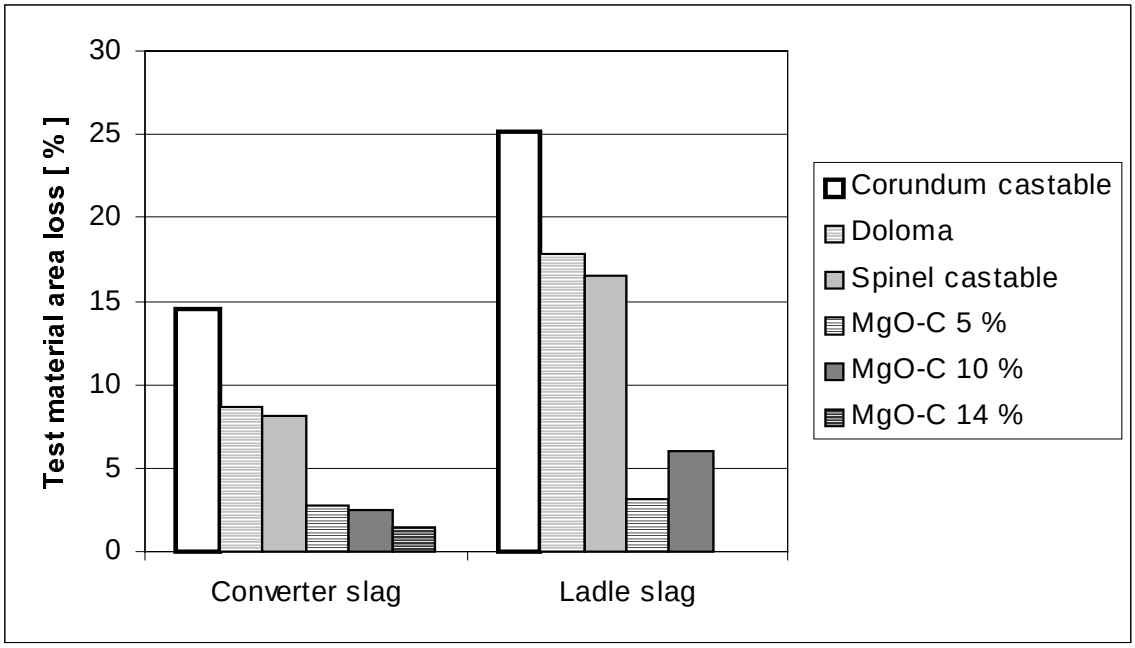

Figure 10. Relative corrosion rate .

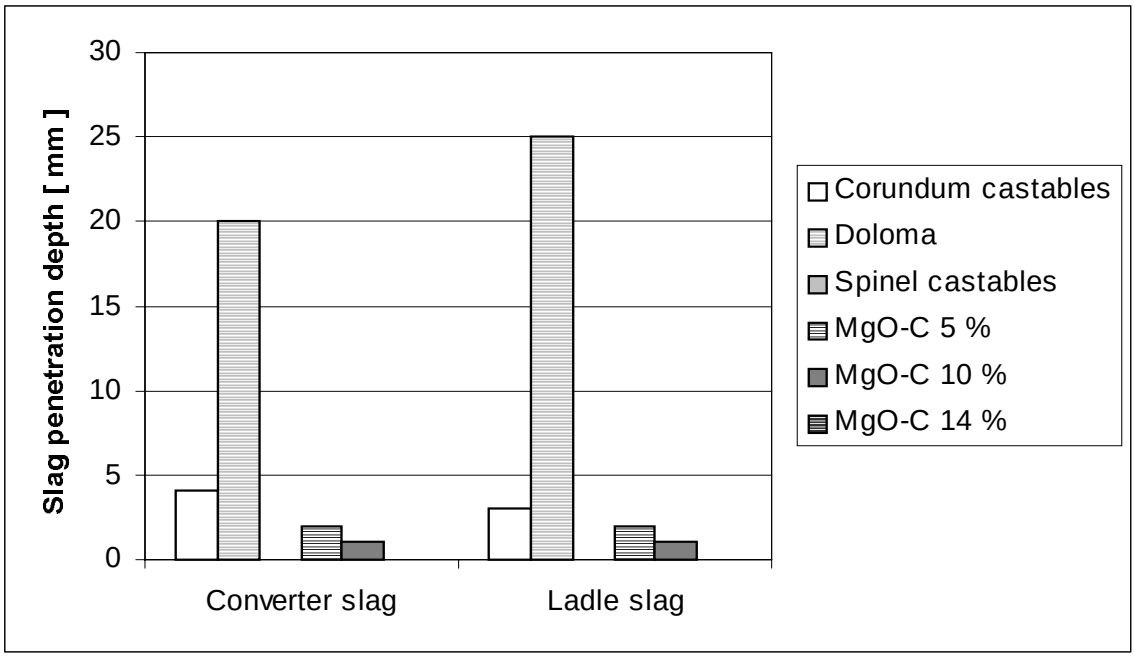

Figure 11. Slag penetration depth into test pieces.

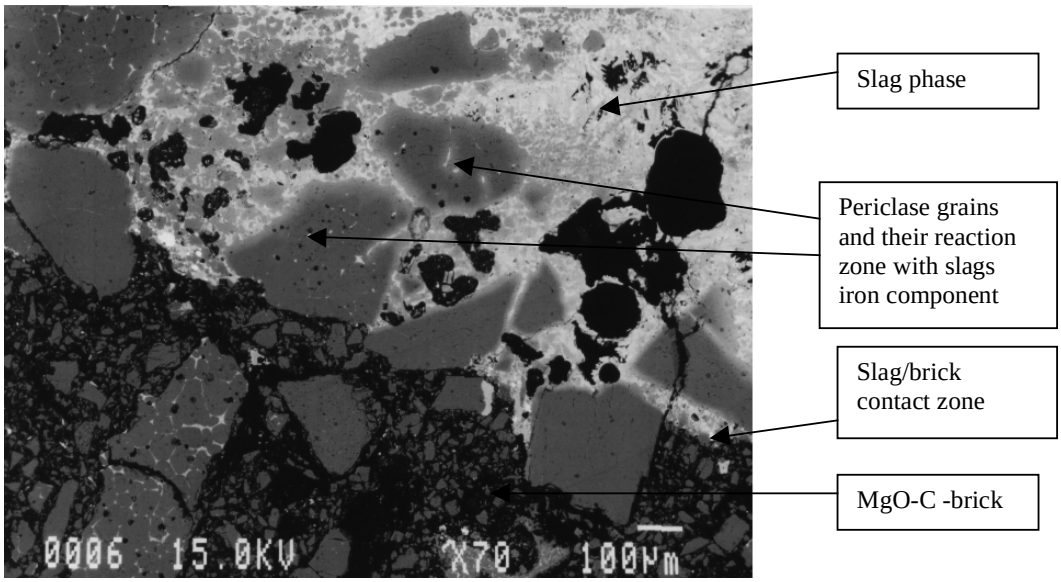

Figure 12. MgO-Carbon (10 % by weight of C) brick and its contact zone with slag.

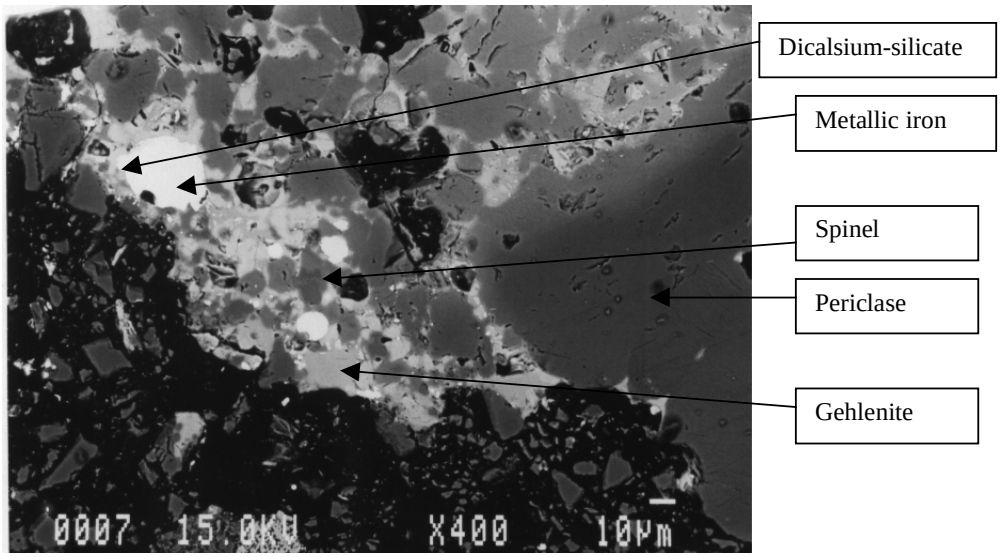

Figure 13. Previous contact zone with magnification of 400.

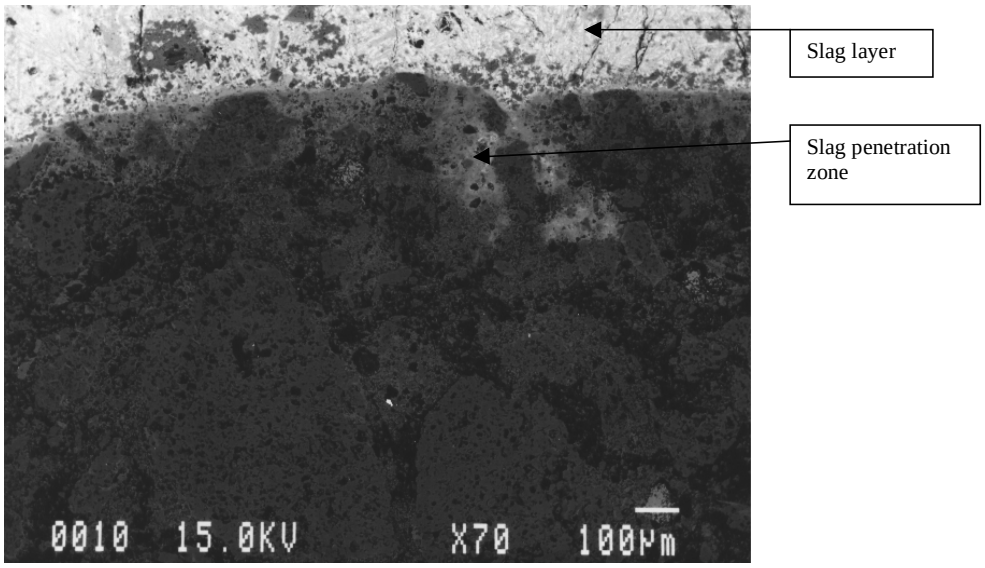

Figure 14. Spinel castable reaction zone with converter slag components.

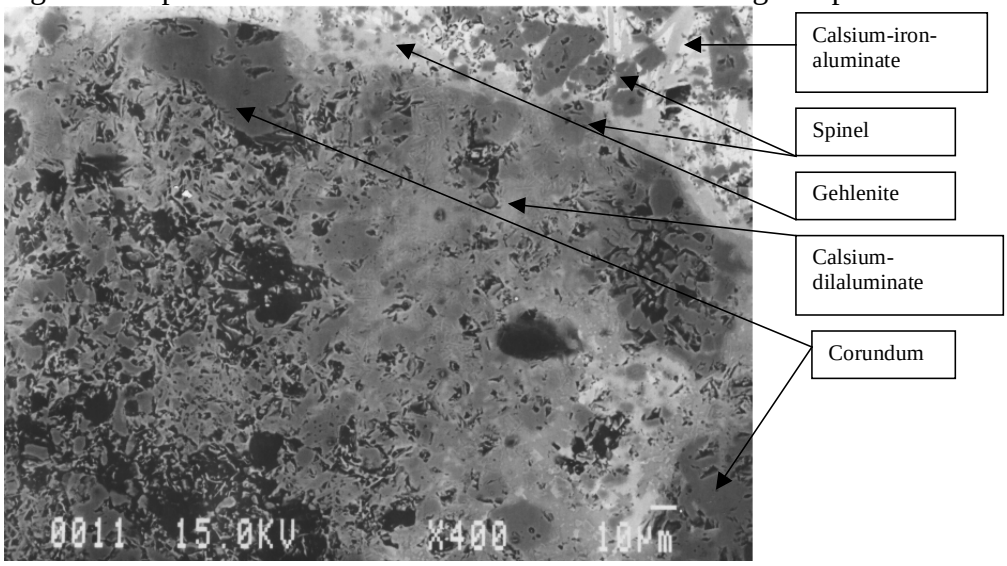

Figure 15. Previous reaction zone with magnification of 400.

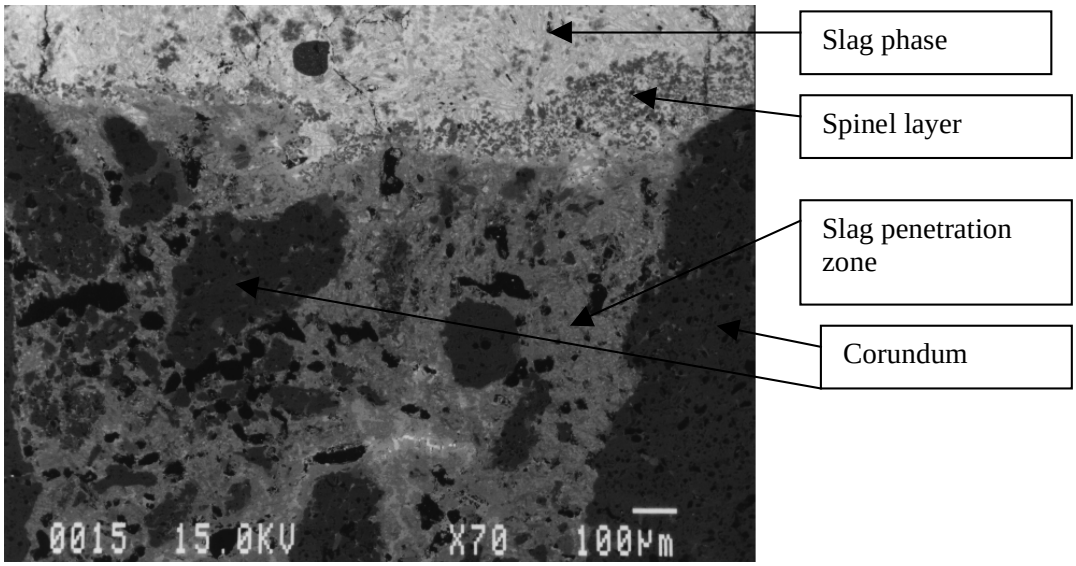

Figure 16. Corundum castable layers and contact zone with converter slag components.

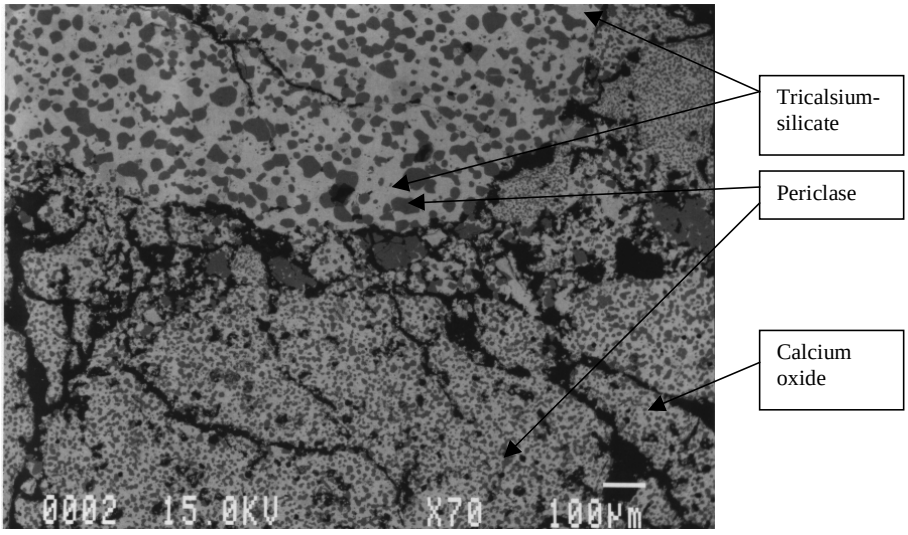

Figure 17. Doloma brick reaction zone with converter slag.

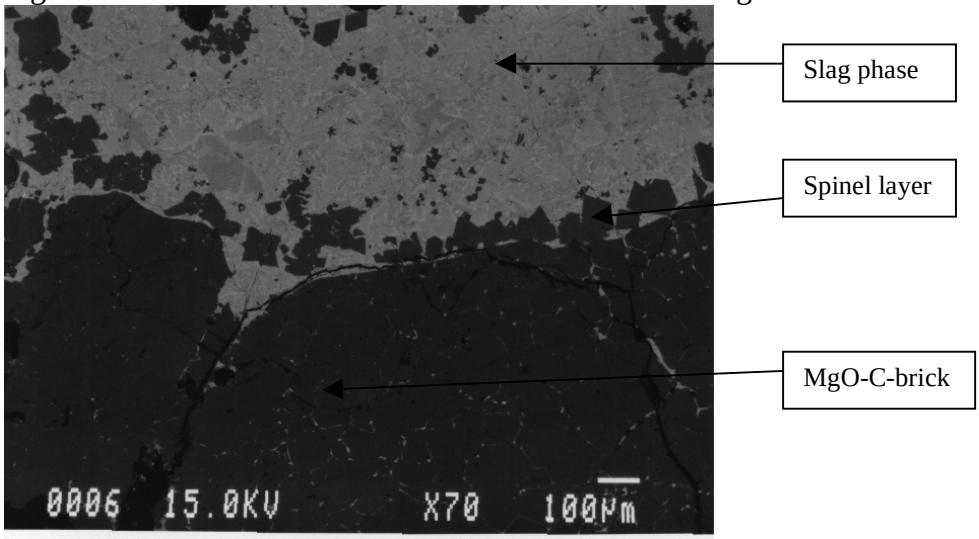

Figure 18. MgO-Carbon (10 %) brick and its reactions with ladle slag components.

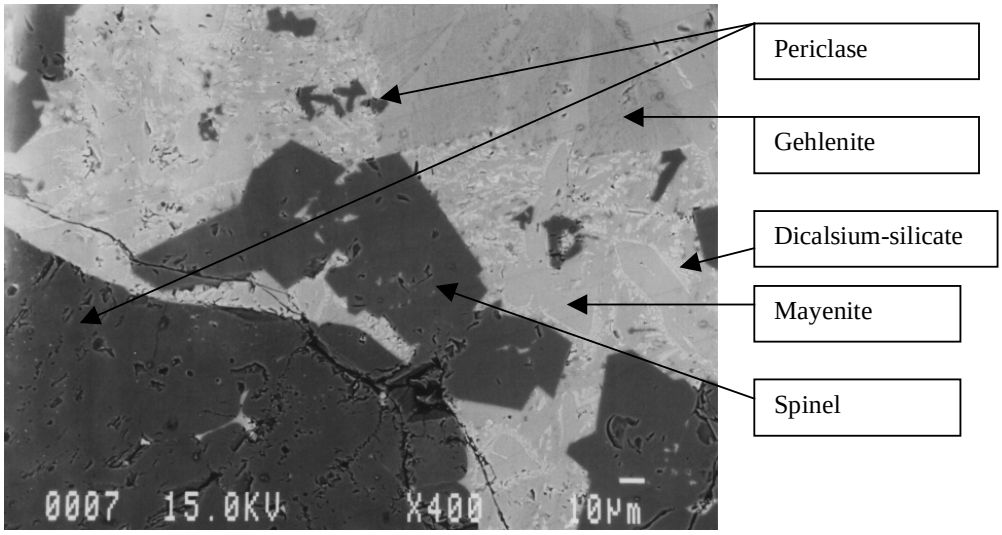

Figure 19. Previous reaction zone with magnification of 400.

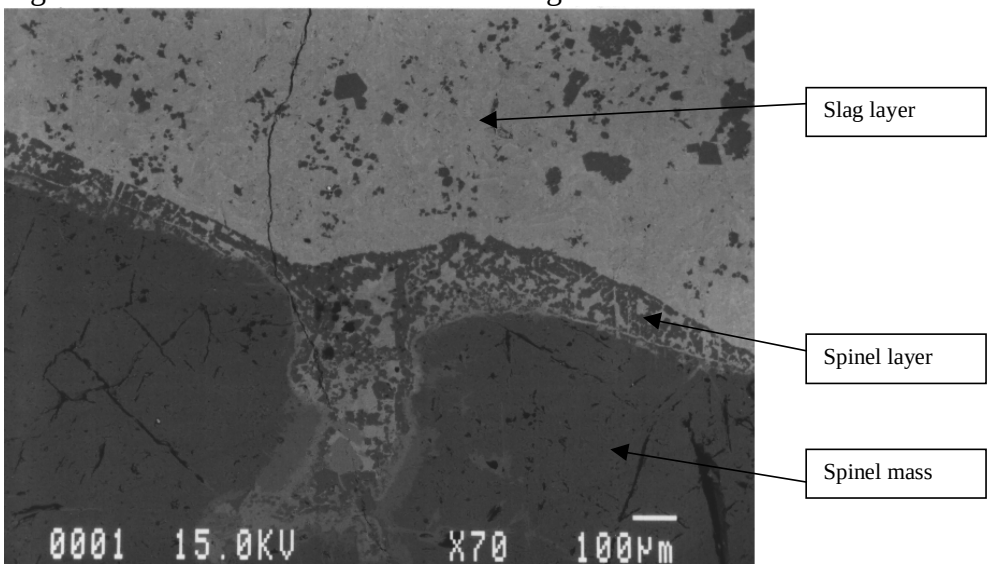

Figure 20. Spinel castable reactions with ladle slag components and formation of spinel layer.

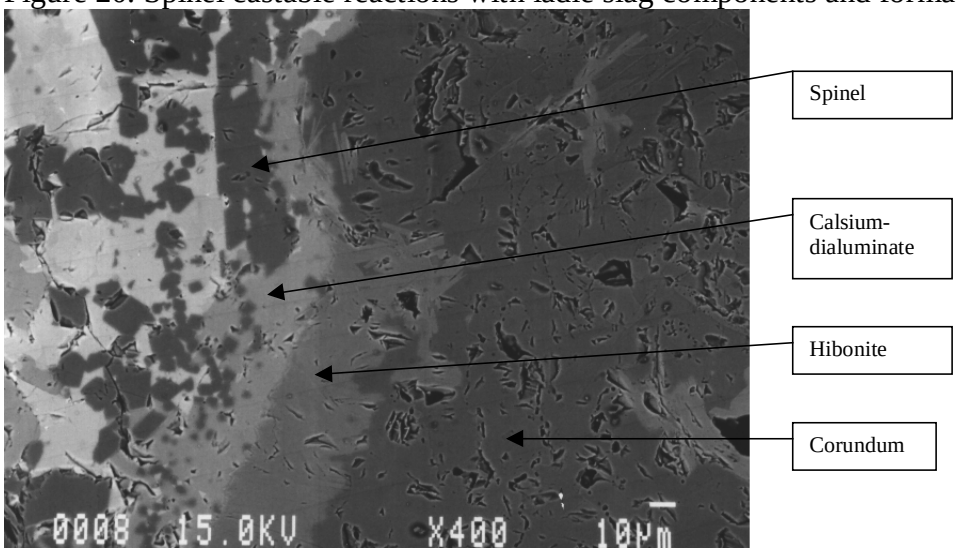

Figure 21. Reaction zone of corundum grain and ladle slag components.

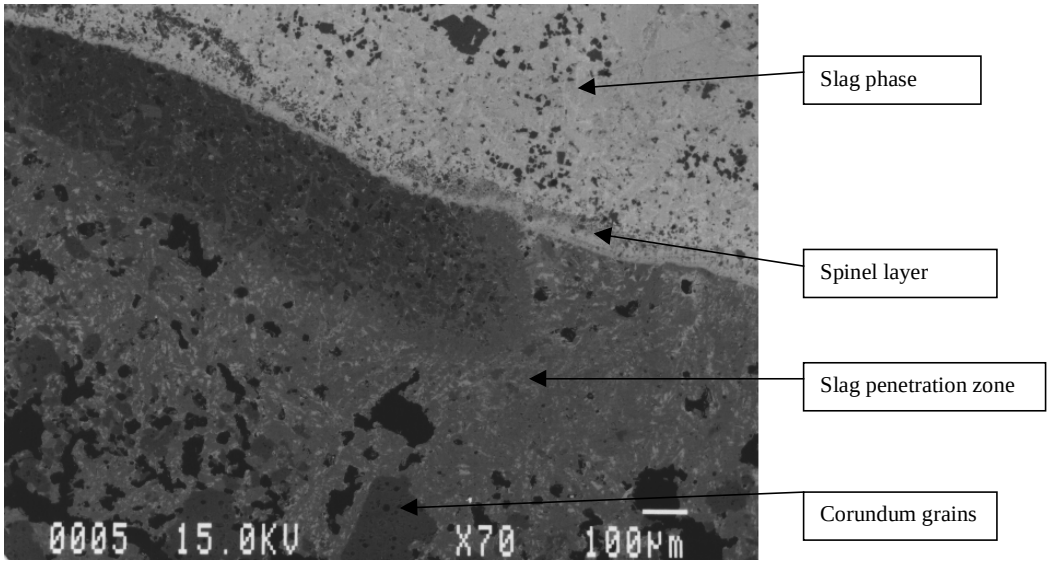

Figure 22. Corundum castable layers with ladle slag components.

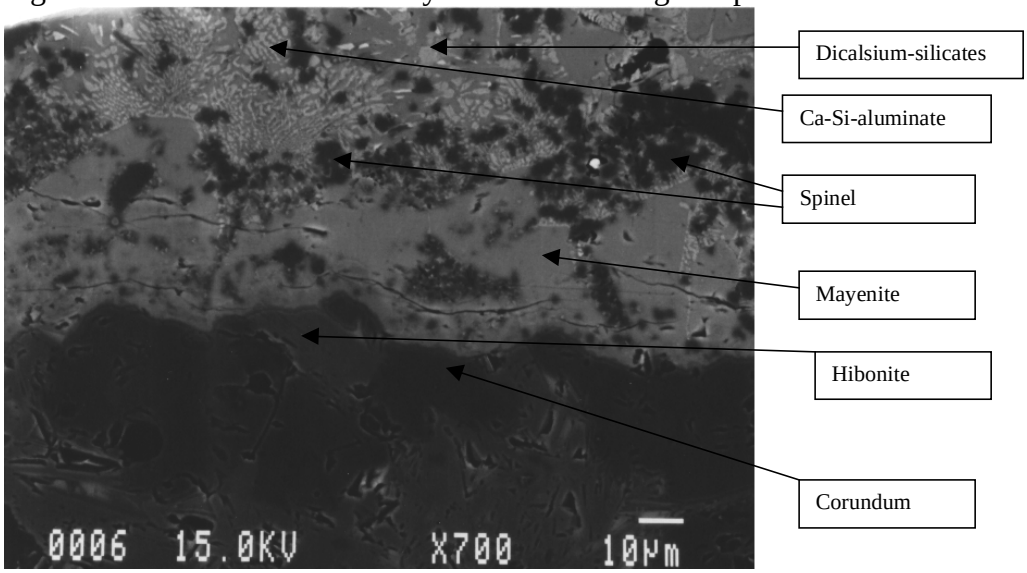

Figure 23. Corundum grain reaction zones with ladle slag.

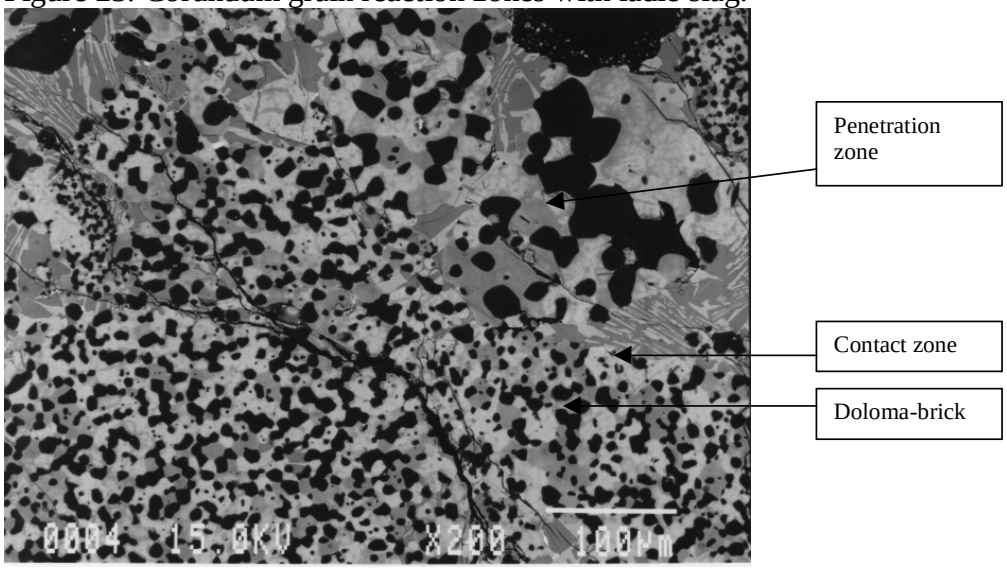

Figure 24. Doloma brick and ladle slag penetration.

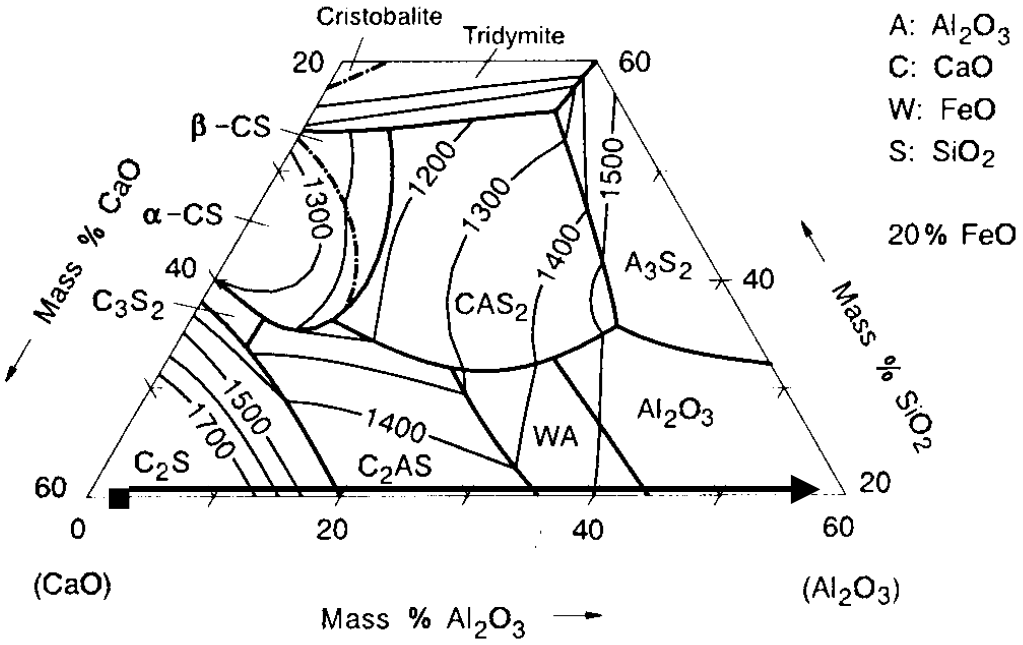

Figure 25. Phase diagram FeO 20 % -Al_2O_3-CaO-SiO_2. ■ = converter slag composition.

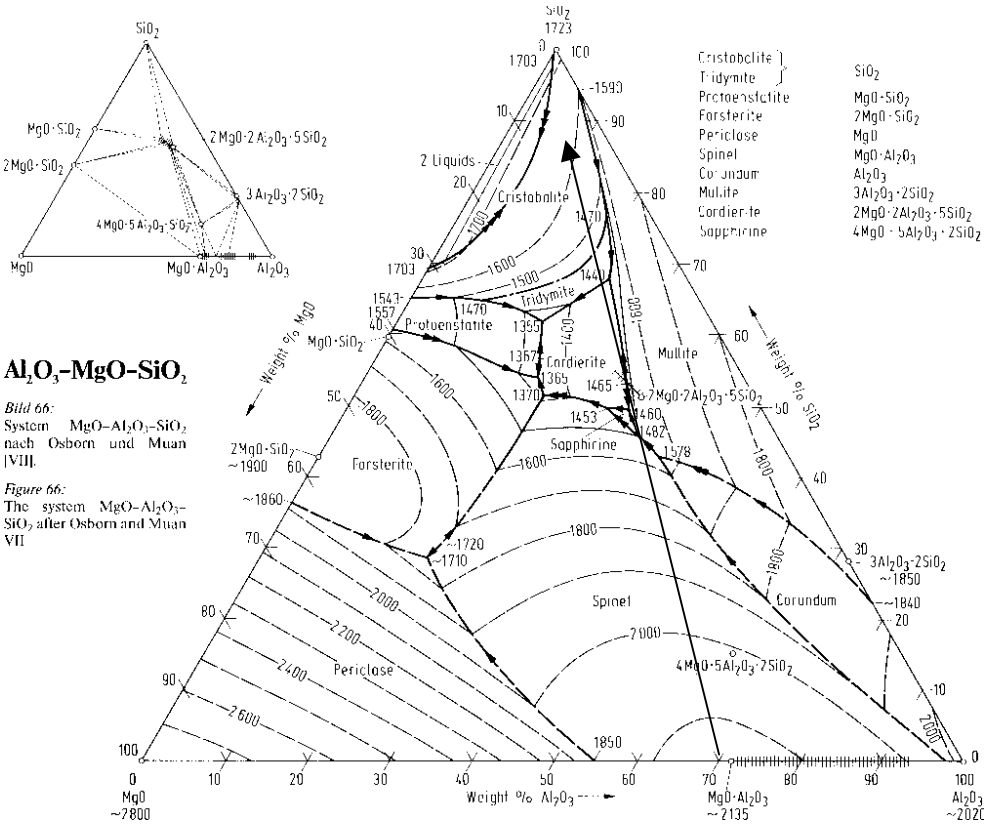

Figure 26. Phase diagram Al_2O_3-MgO-SiO_2.

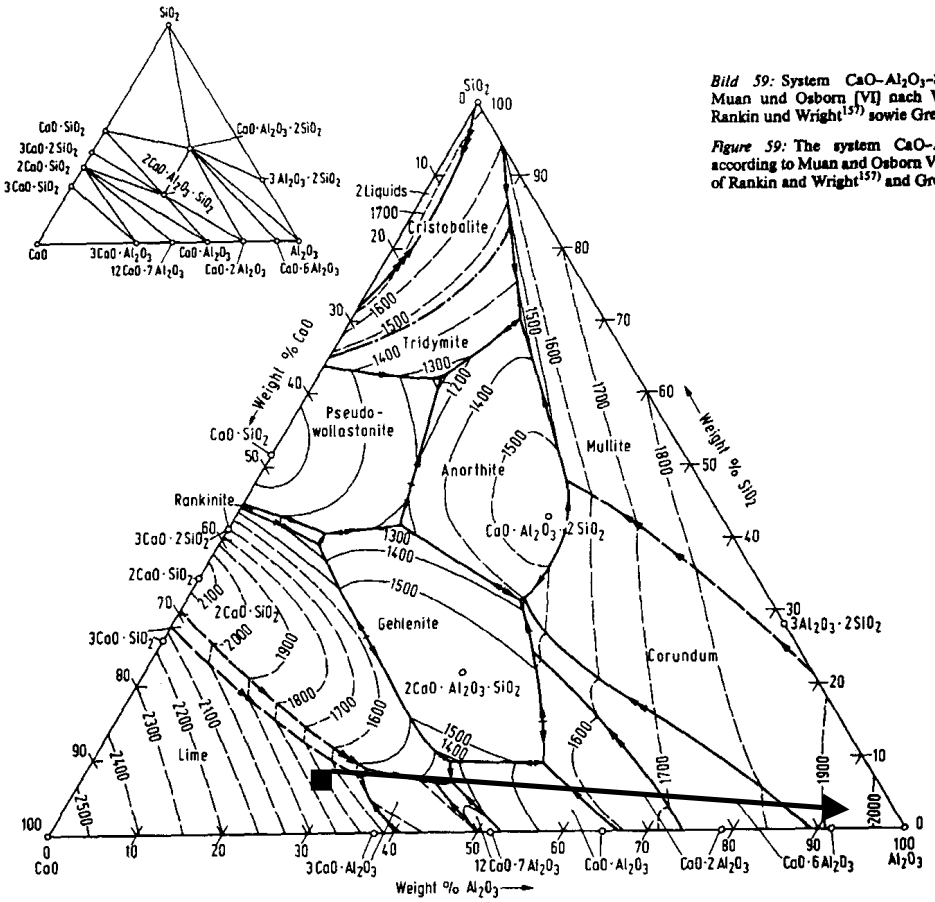

Bild 59: System $CaO-Al_2O_3-SiO_2$ nach Muan und Osborn [VI] nach Werten von Rankin und Wright[157] sowie Greig[158]

Figure 59: The system $CaO-Al_2O_3-SiO_2$ according to Muan and Osborn VI using data of Rankin and Wright[157] and Greig[158]

Figure 27. Phase diagram Al_2O_3-CaO-SiO_2. ■ = ladle slag composition.

CaO-FeO_x

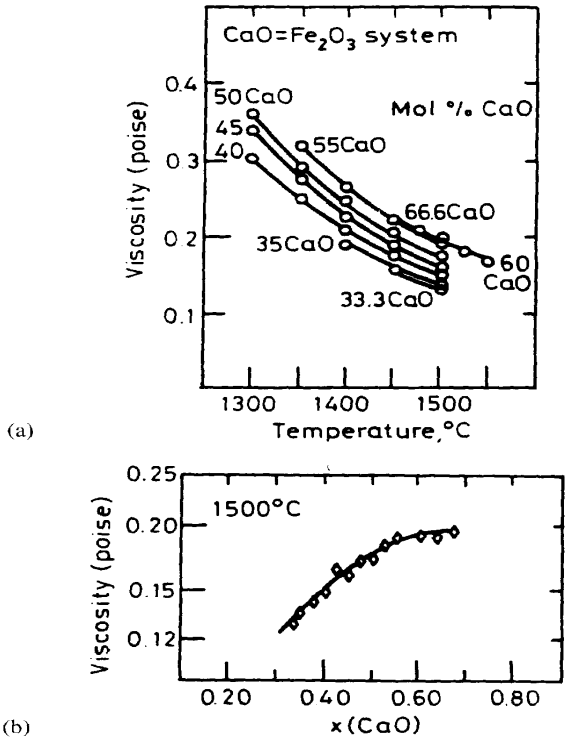

Figure 28. Viscosity's of $CaO-Fe_2O_3$ melts as a function of a) temperature b) composition.

CaO-FeO_x-SiO_2

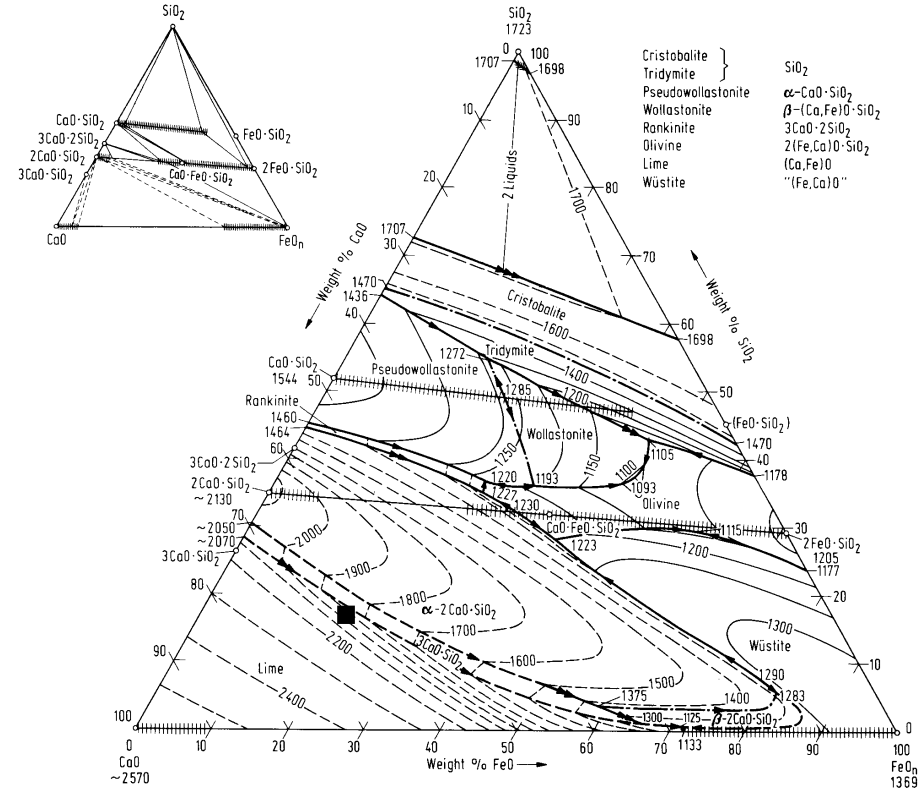

Figure 29. Phase diagram $CaO-FeO-SiO_2$. ■ = converter slag composition.

Table 1. Starting values for the calculations of HSC equilibrium diagrams. Ladle slag.

Chemical components	MgO-C brick (w-%)	Spinel castable (w-%)	Corundum castable (w-%)	Doloma brick (w-%)
Ladle slag				
Al_2O_3	25.2	25.6	25.6	25.6
CaO	63.9	64.9	64.9	64.9
SiO_2	7.3	7.4	7.4	7.4
MgO	2.2	2.2	2.2	2.2
FeO	0.67			
MnO	0.3			
TiO_2	0.5			
Refractory materials				
CaO				71.4
MgO	98			28.6
$2CaO*SiO_2$	2			
Al_2O_3		66.7	66.7	
$MgO*Al_2O_3$		26.7		
$CaAl_{12}O_{19}$		6.7	26.7	
Al_2SiO_5			6.7	

Table 2. Starting values for the calculations of HSC equilibrium diagrams. Converter slag.

Chemical components	MgO-C brick (w-%)	Spinel castable (w-%)	Corundum castable (w-%)	Doloma brick (w-%)
Converter slag				
Al_2O_3	1.1	1.1	1.1	1.1
CaO	57.9	57.9	57.9	57.9
SiO_2	14.2	14.2	14.2	14.2
MgO	1.4	1.4	1.4	1.4
FeO	18.4	18.4	18.4	18.4
MnO	3.1	3.1	3.1	3.1
V_2O_5	2.1	2.1	2.1	2.1
TiO_2	1.7	1.7	1.7	1.7
Refractory materials				
CaO				66.7
MgO	**98**			33.3
$2CaO*SiO_2$	2			
Al_2O_3		80	66.7	
$MgO*Al_2O_3$		15		
$CaAl_{12}O_{19}$		5	26.7	
Al_2SiO_5			6.7	

Table 3. Chemical and physical properties of the test samples. Chemical and physical information is from producers. Mineral analysis by Rautaruukki Steel.

	Spinel castable	Corundum castable	MgO-C 14%	MgO-C 10%	MgO-C 5%	Doloma Brick
Al_2O_3 (w-%) MgO SiO_2 CaO Fe_2O_3 Residual C	95 3,2 0,3 - 0,2 -	97 - 0,6 - 0,1 -	0,3 96,5 0,9 1,8 0,4 14	- 97,2 0,5 1,5 0,5 10	- 97 0,6 1,7 0,4 5	2,0 > 35 < 2,0 < 60 1,5 -
Water addition (w-%)	5,2	6 – 7	-	-	-	-
Thermal conductivity (W/m°K)	2,8 400°C 2,15 800°C 2,2 1200°C	3,3 400°C 2,7 600°C 2,6 1200°C	-	-	-	-
Density g/cm^3	3,04	2,9	2,98	3,05	3,06	-
Porosity %	-	-	<11	4	5	-
CCS N/mm^2	50	80	>20	28,9	40	-
Application	Ladle	Ladle	Ladle	Ladle	Ladle	Ladle
Max temp. °C	1800	1800	-	-	-	-
Physical state	Mass	Mass	Brick	Brick	Brick	Brick
Mineral phases	corundum spinel hibonite	corundumh ibonite kyanite	periclase graphite	periclase graphite calcium aluminium iron oxide	periclase graphite monticellite	Periclase, lime

Table 4. Chemical compositions of slag used in tests.

	Al_2O_3 %	CaO %	SiO_2 %	MgO %	Fe %	Mn %	V %	Ti %	CaO/ SiO_2
Ladle slag	24,6	62,4	7,1	2,1	0,5	0,2	0,0	0,3	8,8
Converter slag	1,1	56,5	13,9	1,4	14,1	2,7	1,6	1,0	4,1

Table 5. Statistic of the tests conditions.

	Test 1	Test 2
Test duration	7 h 40 min	12 h 30 min
Slag were melt in furnace	5 h 25 min	8 h 35 min
One test piece / melt slag contact time	3 h 36 min	5 h 43 min
Average temperature	1500 °C	1500 °C
Slag amount	7 kg	20 kg
Slag type	Converter slag	Ladle slag
Furnace type	Conduct	Conduct

Table 6. Chemical and mineralogical analysis of the converter slag tests (test 1). MgO-C 5 (%) and MgO-C 10 (%).

	MgO-C 5			MgO-C 10		
Chemical analysis (wt-%)	Penetration zone 0-15 mm	Penetration zone 15-30 mm	Initial mass content	Penetration zone 0-15 mm	Penetration zone 15-30 mm	Initial mass content
Al_2O_3 %	1.8	0.2	0.1	3.2	0.6	0.1
MgO %	88	91.8	90.8	86.7	90.9	86.7
SiO_2 %	1	0.6	0.7	1	0.7	0.4
CaO %	3.3	1.8	1.6	3.3	1.6	1.3
Fe_2O_3 %	1.2	0.5	0.4	1.2	0.3	0.3
Cr_2O_3	0.02	0.01	0.01	0.03	0.01	0.01
MnO	0.2	0.03	0.03	0.2	0.02	0.02
Evaporated components	4.21	5.34	6.18	4.03	5.79	11
Mineral phases	Periclase, ringwoodite, graphite, monticellite	Periclase, graphite, monticellite	Periclase, graphite, monticellite	Periclase, ringwoodite, graphite, spinel, monticellite	Periclase, graphite	Periclase, graphite, calcium aluminium iron oxide

Table 7. Chemical and mineralogical analysis of the converter slag tests (test 1). MgO-C 14 (%) and doloma.

	MgO-C 14			Doloma		
Chemical analysis (wt-%)	Penetration zone 0-15 mm	Penetration zone 15-30 mm	Initial mass content	Penetration zone 0-30 mm	Penetration zone 30-50 mm	Initial mass content
Al_2O_3	0.4	0.3	0.3	4.1	0.4	0.4
MgO	84.1	83.9	82.9	37.7	40.4	41.6
SiO_2	0.7	0.6	0.6	1.8	1.1	0.7
CaO	1.6	1.6	1.5	53.4	56.9	56
Fe_2O_3	0.4	0.4	0.4	2.2	0.7	0.7
Cr_2O_3	0.01	0.02	0.01	0.01	0.02	0
MnO	0.03	0.03	0.03	0.3	0.1	0.1
Evaporated components	12.7	13	14.1	-	-	-
Mineral phases	Periclase, graphite, monticellite	Periclase, graphite, monticellite	Periclase, graphite	Periclase, lime, mayenite	Periclase, lime	Periclase, lime, portlandite

Table 8. Chemical and mineralogical analysis of the converter slag tests (test 1). Spinel castable and corundum castable.

	Spinel			Corundum		
Chemical analysis (wt-%)	Penetration zone 0-15 mm	Penetration zone 15-30 mm	Initial mass content	Penetration zone 0-15 mm	Penetration zone 15-30 mm	Initial mass content
Al_2O_3	93.2	93.8	92.5	91.8	95.3	91.8
MgO	3.6	3.9	3.4	0.7	0.1	0.2
SiO_2	0.3	0.1	0.2	1.7	1.2	1.4
CaO	2.1	1.7	1.6	4.2	2.1	2.5
Fe_2O_3	0.3	0.1	0.1	0.8	0.1	0.1
Cr_2O_3	0.01	0	0.01	0.01	0.01	0
MnO	0.03	0	0	0.1	0	0
Evaporated components	0.03	0.06	1.91	0.01	0.34	3.62
Mineral phases	Corundum, spinel, hibonite, merwinite	Corundum, spinel, merwinite hibonite	Corundum, spinel, hibonite	Corundum, spinel, merwinite, hibonite, aluminium silicate	Corundum, spinel, hibonite, merwinite, aluminium silicate	Corundum, hibonite, kyanite

Table 9. Chemical and mineralogical analysis of the ladle slag tests (test 2). MgO-C 5 (%) and MgO-C 10 (%).

	MgO-C 5			MgO-C 10		
Chemical analysis (wt-%)	Penetration zone 0-15 mm	Penetration zone 15-30 mm	Initial mass content	Penetration zone 0-15 mm	Penetration zone 15-30 mm	Initial mass content
Al_2O_3 %	4	0.4	0.1	4.1	0.6	0.1
MgO %	84	93.7	90.8	83.4	90.5	86.7
SiO_2 %	1.5	0.7	0.7	1.4	0.7	0.4
CaO %	5.7	1.9	1.6	5.7	1.6	1.3
Fe_2O_3 %	0.5	0.4	0.4	0.4	0.3	0.3
Cr_2O_3	0.01	0.01	0.01	0.02	0.02	0.01
MnO	0.1	0.03	0.03	0.04	0.02	0.02
Evaporated components	4.09	2.67	6.18	4.82	6.16	11
Mineral phases	Periclase, spinel, mayenite, graphite, gehlenite	Periclase, graphite, mayenite	Periclase, graphite, monticellite	Periclase, graphite, spinel, mayenite, gehlenite, monticellite	Periclase, graphite, mayenite	Periclase, graphite, calcium aluminium iron oxide

Table 10. Chemical and mineralogical analysis of the ladle slag tests (test 2). MgO-C 14 (%) and doloma.

	MgO-C 14			Doloma		
Chemical analysis (wt-%)	Penetration zone 0-15 mm	Penetration zone 15-30 mm	Initial mass content	Penetration zone 0-50 mm	Penetration zone 50-70 mm	Initial mass content
Al_2O_3	7.9	0.4	0.3	7.6	2.4	0.4
MgO	70.9	83	82.9	32.2	38.4	41.6
SiO_2	2	0.7	0.6	2.4	1.5	0.7
CaO	8.3	1.6	1.5	54.7	56.7	56
Fe_2O_3	0.5	0.4	0.4	1	0.9	0.7
Cr_2O_3	0.02	0.01	0.01	0.01	0.01	0
MnO	0.1	0.03	0.03	0.1	0.1	0.1
Evaporated components	10.1	13.8	14.1	-	-	-
Mineral phases	Periclase, spinel, graphite, mayenite, gehlenite	Periclase, graphite, mayenite	Periclase, graphite	Periclase, lime, mayenite, calcium silicate, portlandite, calcite	Periclase, lime, portlandite	Periclase, lime, portlandite

Table 11. Chemical and mineralogical analysis of the ladle slag tests (test 2). Spinel castable and corundum castable.

	Spinel			Corundum		
Chemical analysis (wt-%)	Penetration zone 0-15 mm	Penetration zone 15-30 mm	Initial mass content	Penetration zone 0-15 mm	Penetration zone 15-30 mm	Initial mass content
Al_2O_3	81	94	92.5	90.1	96	91.8
MgO	7.3	3.6	3.4	1.5	0.1	0.2
SiO_2	1.6	0.1	0.2	1.8	1.1	1.4
CaO	9	1.7	1.6	5.6	2.1	2.5
Fe_2O_3	0.8	0.1	0.1	0.3	0.2	0.1
Cr_2O_3	0.02	0.01	0.01	0.01	0.01	0
MnO	0.03	0	0	0.01	0	0
Evaporated components	0.14	0.14	1.91	0.03	-	3.62
Mineral phases	Periclase, corundum, mayenite, spinel, hibonite	Corundum, spinel, hibonite,	Corundum, spinel, hibonite	Corundum, spinel, calcium aluminium oxide, merwinite	Corundum, calcium silicate hydrate, hibonite	Corundum, hibonite, kyanite